Acta Crystallographica Section F
Structural Biology Communications
ISSN 2053-230X

Crystallization and preliminary X-ray crystallographic analysis of the C-terminal domain of guanylate kinase-associated protein from *Rattus norvegicus*

Junsen Tong, Huiseon Yang and Young Jun Im*

College of Pharmacy, Chonnam National University, Gwangju 500-757, Republic of Korea

Correspondence e-mail: imyoungjun@jnu.ac.kr

Received 4 February 2014
Accepted 22 May 2014

Guanylate kinase-associated protein (GKAP) is a scaffolding protein that plays a role in protein–protein interactions at the synaptic junction such as linking the NMDA receptor–PSD-95 complex to the Shank–Homer complex. In this study, the C-terminal helical domain of GKAP from *Rattus norvegicus* was purified and crystallized by the vapour-diffusion method. To improve the diffraction quality of the GKAP crystals, a flexible loop in GKAP was truncated and an MBP (maltose-binding protein)-GKAP fusion was constructed in which the last C-terminal helix of MBP is fused to the N-terminus of the GKAP domain. The MBP-GKAP crystals diffracted to 2.0 Å resolution using synchrotron radiation. The crystal was orthorhombic, belonging to space group $P2_12_12$, with unit-cell parameters a = 99.1, b = 158.7, c = 65.5 Å. The Matthews coefficient was determined to be 2.44 Å^3 Da^{-1} (solvent content 49.5%) with two molecules in the asymmetric unit. Initial attempts to solve the structure by molecular replacement using the MBP structure were successful.

1. Introduction

Synaptic function depends on the proper localization of various ion channels, receptors and signalling molecules in the synapse. Targeting of these molecules is mediated by their interactions with specific intracellular anchoring or clustering proteins (Naisbitt *et al.*, 1997). The postsynaptic density (PSD) is an electron-dense structure associated with the cytoplasmic face of the postsynaptic membrane. The PSD consists of a network of proteins that link glutamate receptors and other postsynaptic proteins to the cytoskeleton and signalling pathways in the excitatory synapses (Sheng & Hoogenraad, 2007). GKAPs (guanylate kinase-associated proteins) [also known as discs-large-associated 43 protein (DAP) family proteins] are a family of scaffold proteins that were initially identified by their interaction with the guanylate kinase (GK) domain of postsynaptic density protein-95 (PSD-95; Kim *et al.*, 1997). GKAP interacts with various binding partners such as synaptic scaffolding molecule (Hirao *et al.*, 1998), Shank (Naisbitt *et al.*, 1999), dynein light chain (Naisbitt *et al.*, 2000) and discs-large homologue 1 (Manneville *et al.*, 2010). By these interactions, GKAP physically links the *N*-methyl-D-aspartic acid (NMDA) receptor–PSD-95 complex to the type I metabotropic glutamate receptor–Homer complex and to motor proteins (Tu *et al.*, 1999).

There are at least six alternative splicing variants of GKAP in *Rattus norvegicus* and seven variants in humans (Kim *et al.*, 1997). GKAP family proteins are characterized by the presence of a GKAP homology domain (GH) in the C-termini of these proteins (Naisbitt *et al.*, 1997; Kim *et al.*, 1997). The longest isoform, GKAP1 in rat, is composed of 992 amino acids. The N-terminal 800 residues are predicted to be unstructured, while the C-terminal GKAP homology domain is predicted to be composed of four α-helices. GKAP binding to Shank proteins is mediated by a short C-terminal PDZ-binding sequence common to all GKAP splice variants (Naisbitt *et al.*, 1999). GKAP binding to the GK domain of PSD-95 is mediated by the N-terminal region containing multiple 14-amino-acid repeats that are

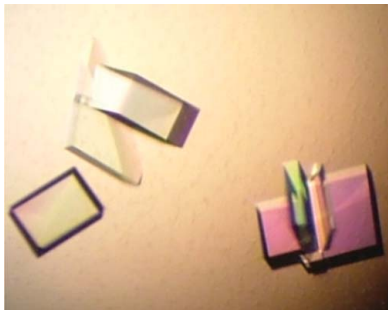

conserved in all GKAP proteins (Kim *et al.*, 1997). Stimulating neuronal activity induces the ubiquitination and degradation of GKAP and Shank, while inactivity induces synaptic accumulation of GKAP (Hung *et al.*, 2010; Shin *et al.*, 2012). The biochemical changes at synapses accompanied by chronic activity modulation by the ubiquitin–proteasome system provide a potential molecular mechanism for homeostatic plasticity (Shin *et al.*, 2012). However, the molecular mechanisms of GKAP regulating the postsynaptic targeting and remodelling of receptors and scaffolding proteins in the PSD are still largely unknown.

The GKAP homology domain composed of 170 residues has no recognizable similarity to any characterized protein domains and has no homology to the proteins of known structures in the Protein Data Bank. However, the conservation of this region across the GKAP homologues and the presence of predicted α-helical structures indicate that the GH domain may represent a discrete domain with functional significance. In order to obtain structural insight into the role of GKAP, we initiated crystallographic studies of the GKAP homology domain. Here, we report the purification, crystallization and X-ray data collection of GKAP GH from *R. norvegicus*.

2. Materials and methods

2.1. Cloning and protein expression

DNA encoding the C-terminal GH domain (residues 807–971) of GKAP (UniProt ID P97836) was amplified by polymerase chain reaction (PCR) using cloned GKAP DNA from *R. norvegicus*. The C-terminal PDZ-binding motif (residues 987–992) was not included in the constructs. The GKAP GH DNA was amplified using the oligonucleotide primers 5′-GAGCTCGCCATGGACGGCCAC-TGGTTCC-3′ (forward) and 5′-CATTATCTCGAGTCACTGGCG-GACTGATGCTG-3′ (reverse). The PCR product was subcloned into the *Nco*I and *Xho*I sites of a modified pHIS-parallel2 vector. GKAP was tagged with an N-terminal hexahistidine followed by a thrombin protease cleavage site (LVPR/GS). The GKAP GH domain is predicted to contain four α-helices based on secondary-structure prediction. The long α3-α4 loop is composed of 40 residues and is rich in arginine, lysine and proline residues (Fig. 1). We observed significant proteolytic degradation in the α3-α4 loop during protein expression and thrombin treatment owing to disorder of the loop. To improve the crystallization properties of the GKAP construct, the 29 residues (residues 917–945) in the α3-α4 loop were replaced by a dipeptide sequence (Val-Asp) of the *Sal*I restriction-enzyme recognition sequence by PCR-based mutagenesis using the following pair of primers: 5′-CTAGATAGTCGACCGCTCGCTGGAGAGCTC-3′ (sense), 5′-CTAGATAGTCGACCTGTTTCCAATTATTGG-3′ (antisense). The PCR product amplified from the pHIS-*GKAP GH* using the indicated primers was digested with the *Sal*I restriction enzyme and self-ligated to generate the loop truncation. Open reading frames of all mutant genes were confirmed by DNA sequencing.

To produce fusion constructs of His-MBP (MBP = maltose-binding protein) and GKAP, DNA of the loop-truncated GKAP GH was subcloned into the *Nco*I and *Xho*I sites of modified pHIS-MBP vectors. The MBP (UniProt ID P0AEX9) was modified to lack the last few residues in the C-terminal α-helix compared with wild-type MBP. The last residue numbers of MBPs used for the fusion proteins were 389 (MBP1) and 387 (MBP2). The N-terminus of GKAP was connected to the MBPs with a two-amino-acid linker originating from the *Nco*I recognition sequence. The modification of MBP was designed to minimize the flexibility of the connecting loop between MBP and GKAP. The MBP-GKAP constructs used for protein expression had the following amino-acid sequence: MSYYHHHHHHDAS-LVPRGS (thrombin cleavage site)-MBP (residues 28–389 or 28–387)-AM (from the multiple cloning site)-GKAP (residues 807–916)-VD (*Sal*I site)-GKAP (residues 946–971). The pHIS-*GKAP GH* and pHIS-MBP-*GKAP GH* (residues 807–971, 917–945Δ) were transferred into *Escherichia coli* strain BL21(DE3) cells. Transformed cells were grown to an OD_{600} of 0.8 at 310 K in Luria–Bertani medium and protein expression was induced by the addition of 0.5 m*M* isopropyl β-D-1-thiogalactopyranoside. The culture was incubated for 12 h at 293 K before harvesting the cells.

2.2. Protein purification

Cells expressing His-tagged GKAP GH were resuspended in lysis buffer (2× PBS buffer supplemented with 20 m*M* imidazole) and lysed by sonication. Cell lysates were centrifuged at 13 000 rev min^{-1} for 45 min. The supernatant containing His-GKAP was applied onto an Ni–NTA affinity column. The Ni–NTA column was thoroughly washed with the lysis buffer. The protein was eluted from the column using 0.1 *M* Tris–HCl pH 7.0, 0.3 *M* imidazole, 0.3 *M* NaCl. The eluate was concentrated to 10 mg ml^{-1} and the His tag was removed by cleavage with thrombin protease. GKAP GH was subjected to size-exclusion chromatography on a Superdex 200 column (GE Healthcare) equilibrated with 20 m*M* Tris–HCl pH 7.5, 0.1 *M* NaCl. The

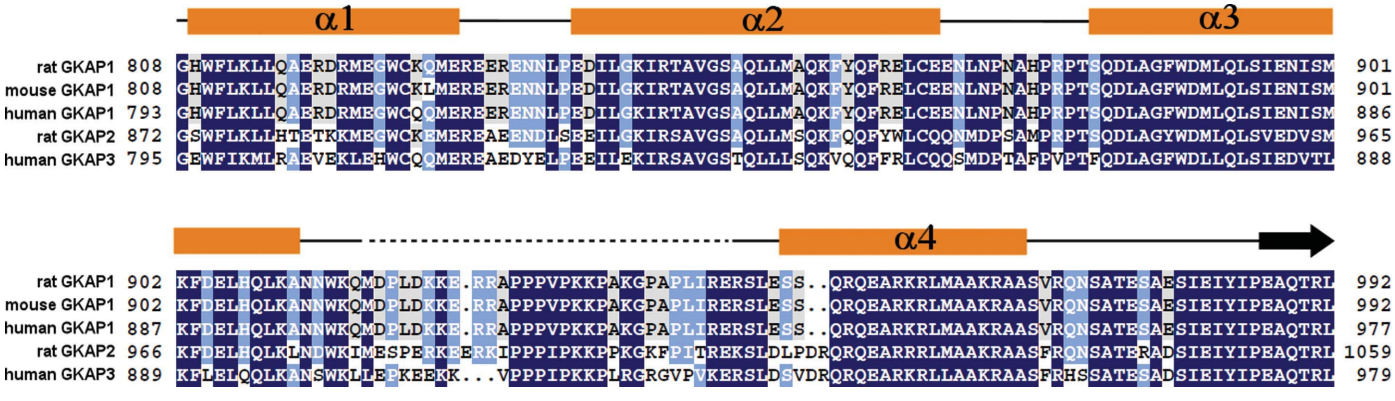

Figure 1
Sequence alignments of the C-terminal GH domains of GKAP homologues. Predicted secondary-structure elements are indicated by rectangles (https://www.predictprotein.org/). Truncation of the α3-α4 loop is indicated by a dotted line. The PDZ-binding motif is shown with an arrow.

Table 1
Summary of diffraction data statistics.

Values in parentheses are for the highest resolution shell.

Crystal	MBP1-GKAP	MBP2-GKAP
Wavelength (Å)	0.97949	0.97857
X-ray source	PLS-5C	PLS-7A
Space group	$P2_1$	$P2_12_12$
Oscillation angle per image (°)	0.5	1
Rotation range (°)	140	230
Unit-cell parameters (Å, °)	a = 65.5, b = 152.0, c = 109.4, β = 99.2	a = 99.1, b = 158.7, c = 65.5
Resolution (Å)	50–3.3 (3.36–3.30)	50–2.0 (2.03–2.00)
No. of observed reflections	90851	469641
No. of unique reflections	30218 (1509)	68103 (2793)
Multiplicity	3.0 (3.0)	6.9 (3.9)
$\langle I/\sigma(I)\rangle$	11.9 (3.8)	45.6 (3.9)
$R_{\rm merge}$† (%)	12.9 (32.5)	7.6 (40.9)
Data completeness (%)	95.1 (97.0)	97.1 (80.5)

† $R_{\rm merge} = \sum_{hkl}\sum_i |I_i(hkl) - \langle I(hkl)\rangle| / \sum_{hkl}\sum_i I_i(hkl)$, where $I_i(hkl)$ is the observed intensity and $\langle I(hkl)\rangle$ is the average intensity of symmetry-related observations.

fractions containing GKAP were concentrated to 10 mg ml^{-1} for crystallization. MBP-GKAP constructs were expressed and purified by the same procedures as used for the purification of His-GKAP GH domain (Fig. 2).

2.3. Crystallization

Preliminary crystallization experiments were carried out at 291 K by vapour-diffusion methods using customized crystallization screening solutions. 0.8 µl protein solution and 0.8 µl precipitant solution were dispensed onto 96-well crystallization plates using a multi-channel pipette. Subsequent optimization of the initial crystallization hits was carried out using 15-well screw-cap plates (Qiagen) by the hanging-drop vapour-diffusion method. 2 µl protein solution was mixed with an equal volume of precipitant solution and equilibrated against 1 ml reservoir solution. Partially degraded GKAP GH protein yielded microcrystals of thin hexagonal plates in a few days, while the intact GKAP GH protein did not crystallize (Fig. 3*a*). Crystals of the loop-truncated GKAP GH (residues 807–971, 917–945Δ) grew in 0.1 *M* MES–NaOH pH 6.0, 15% polyethylene glycol (PEG) 4000, 0.2 *M* ammonium sulfate to a typical size of 0.1 mm in length (Fig. 3*b*). X-ray diffraction studies of the GKAP GH (917–945Δ) crystals showed weak diffraction to 5 Å resolution. Extensive attempts to improve the diffraction limits of the crystals by optimizing the crystallization conditions were not successful. As an alternative approach to obtain diffracting crystals, we tested the crystallization of MBP-GKAP chimeric proteins. Crystals of the MBP1-GKAP (residues 807–971, 917–945Δ) were grown in 0.1 *M* sodium citrate pH 5.0, 15% PEG 1500, 0.1 *M* NaCl with a typical size of 0.2 mm in length (Fig. 3*c*). Crystals of the MBP2-GKAP GH were grown in 0.1 *M* sodium citrate pH 5.0, 15% PEG 1500, 0.1 *M* NaCl with a typical size of 0.2 × 0.2 × 0.1 mm by micro-seeding techniques (Fig. 3*d*).

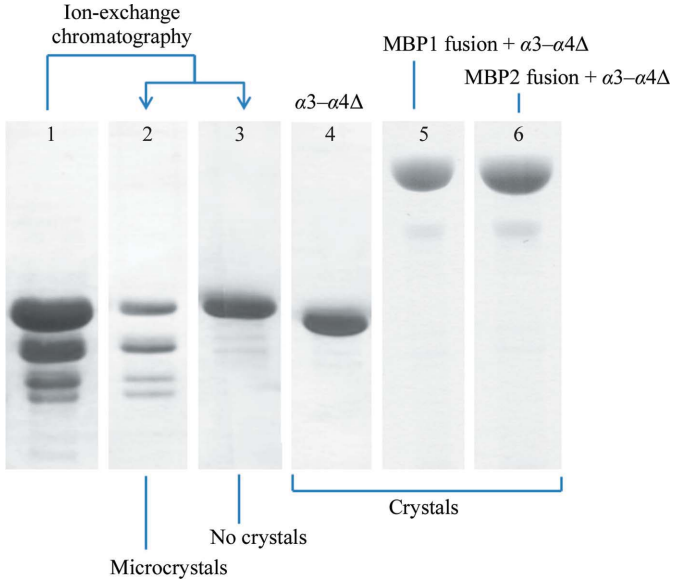

Figure 2
Purified GKAP constructs used for crystallization studies. Lane 1, partially fragmented GKAP GH (residues 807–971) obtained from size-exclusion chromatography. Lane 2, GKAP GH fragments isolated from the protein in lane 1. Lane 3, intact GKAP GH (residues 807–971) separated from the partially fragmented sample of lane 1. Lane 4, the α3-α4 loop-truncated GKAP GH (residues 807–971, Δ917–945). Lane 5, MBP1 (residues 28–389)-GKAP GH (residues 807–971, Δ917–945). Lane 6, MBP2 (residues 28–387)-GKAP GH (residues 807–971, Δ917–945).

2.4. Diffraction experiment

The crystals were cryoprotected by transferring them into reservoir solution supplemented with an additional 10% PEG 1500 and 10%(*v*/*v*) glycerol and were flash-cooled by immersion in liquid nitrogen. The crystals were preserved in a cryogenic nitrogen-gas stream (∼100 K) during diffraction experiments. Diffraction data for MBP1-GKAP were collected at a wavelength of 0.97949 Å using an ADSC Q315 CCD detector on beamline 5C at the Pohang Light Source (PLS-5C), Pohang Accelerator Laboratory, Republic of Korea. Diffraction data for GKAP and MBP2-GKAP crystals were collected at a wavelength of 0.97857 Å using an ADSC Q270 CCD detector on beamline 7A at the Pohang Light Source (PLS-7A). All data were processed and scaled using *HKL*-2000 (Otwinowski & Minor, 1997) and handled with the *CCP*4 program suite (Winn *et al.*, 2011). Self-rotation analysis and molecular replacement using the MBP structure (PDB entry 1omp; Sharff *et al.*, 1992) were carried out using *MOLREP* (Vagin & Teplyakov, 2010).

3. Results and discussion

GKAP GH domain was cloned into the vectors providing N-terminal hexahistidine or N-terminal His-MBP tags. The GKAP GH domain (residues 807–971) underwent proteolytic fragmentation by endogenous bacterial proteases during the expression and purification steps. The disordered region which is susceptible to proteolysis was predicted to be the α3-α4 loop spanning residues 912–949 by secondary-structure prediction (Fig. 1). The intact GKAP GH and fragmented GKAP GH were separated by ion-exchange chromatography since the presence of nine basic residues in the α3-α4 loop gave a significant difference of isoelectric points (2.9) between the intact form and the fragmented form lacking the α3-α4 loop (Fig. 2). Intact GKAP GH did not crystallize, while the fragmented GH produced hexagonal microcrystals in the preliminary screenings, suggesting that the flexible α3-α4 loop regions might interfere with the crystallization of GKAP (Fig. 3*a*). Therefore, a part of the α3-α4 loop (residues 917–945) was deleted to obtain stable constructs for crystallization. The deletion construct readily formed crystals with improved morphology in 0.1 *M* MES–NaOH pH 6.0, 15% PEG 4000, 0.2 *M* ammonium sulfate (Fig. 3*b*). Crystals of the loop-truncated construct diffracted to 5 Å resolution using synchrotron radiation, which was not suitable for structure determination (Fig. 4). Preliminary data processing showed the crystal belonged to space group

*C*2, with unit-cell parameters a = 238.6, b = 151.9, c = 142.0 Å, β = 101.1°.

As an alternative approach to improve the diffraction limits of the crystals, we applied an N-terminal MBP fusion technique, which has been successfully exploited in the crystallization of various globular proteins (Moon *et al.*, 2010; Smyth *et al.*, 2003). To minimize the flexibility of the fusion protein caused by hinge movement between the MBP and the GH domain, the number of linker residues between MBP and GKAP GH was limited to two amino-acid residues. The N-terminus of GKAP is predicted to be an α-helix starting at the second residue of the GKAP GH construct. We hypothesized that partial truncation of the C-terminal α-helix of MBP and the use of short linkers might allow the α1 helix of GKAP GH to occupy the truncated region in the MBP, which might facilitate a tight packing of the MBP and the GKAP domain.

Two types of C-terminally truncated MBPs (MBP1, residues 28–389, and MBP2, residues 28–387) were fused to the N-terminus of the loop-truncation mutant of GKAP GH. MBP1-GKAP readily produced crystals of size of 0.2 × 0.05 × 0.02 mm in a few days (Fig. 3*c*). The MBP1–GKAP crystal diffracted to 3.3 Å resolution and belonged to space group $P2_1$. MBP2-GKAP was crystallized in an identical condition to MBP1-GKAP with a more voluminous shape than the MBP1 fusion (Fig. 3*d*). The MBP2-GKAP fusion is two amino acids shorter than the MBP1-GKAP fusion in the C-terminal helix of MBP. MBP2-GKAP displayed a significantly improved diffraction limit of 2.0 Å resolution compared with MBP1-GKAP. The MBP2-GKAP construct consisted of 364 amino acids from MBP and 138 residues from GKAP with a total molecular weight of 56 165 Da as calculated from the primary sequence. A complete diffraction data set was collected to 2.0 Å resolution using a native crystal. Data-collection statistics are shown in Table 1. There were a total of 68 103 unique reflections in the resolution range 50–2.0 Å. Analysis of the diffraction intensities confirmed the space group to be orthorhombic $P2_12_12$, with unit-cell parameters a = 99.1, b = 158.7, c = 65.5 Å. The Matthews coefficient was 2.44 Å^3 Da^{-1} for two copies of MBP2-GKAP in the asymmetric unit with a solvent content of 49.5% (Matthews, 1968). A self-rotation function calculated using 9–3.5 Å resolution data showed peaks of 5.4σ corresponding to a twofold noncrystallographic symmetry axis in the κ = 180° section (Fig. 4*d*), while no dominant features corresponding to a threefold noncrystallographic symmetry (NCS) axis were observed in the κ = 120° section. Based on the Matthews coefficient and the self-rotation, we assumed that the crystals contained two molecules in the asymmetric unit.

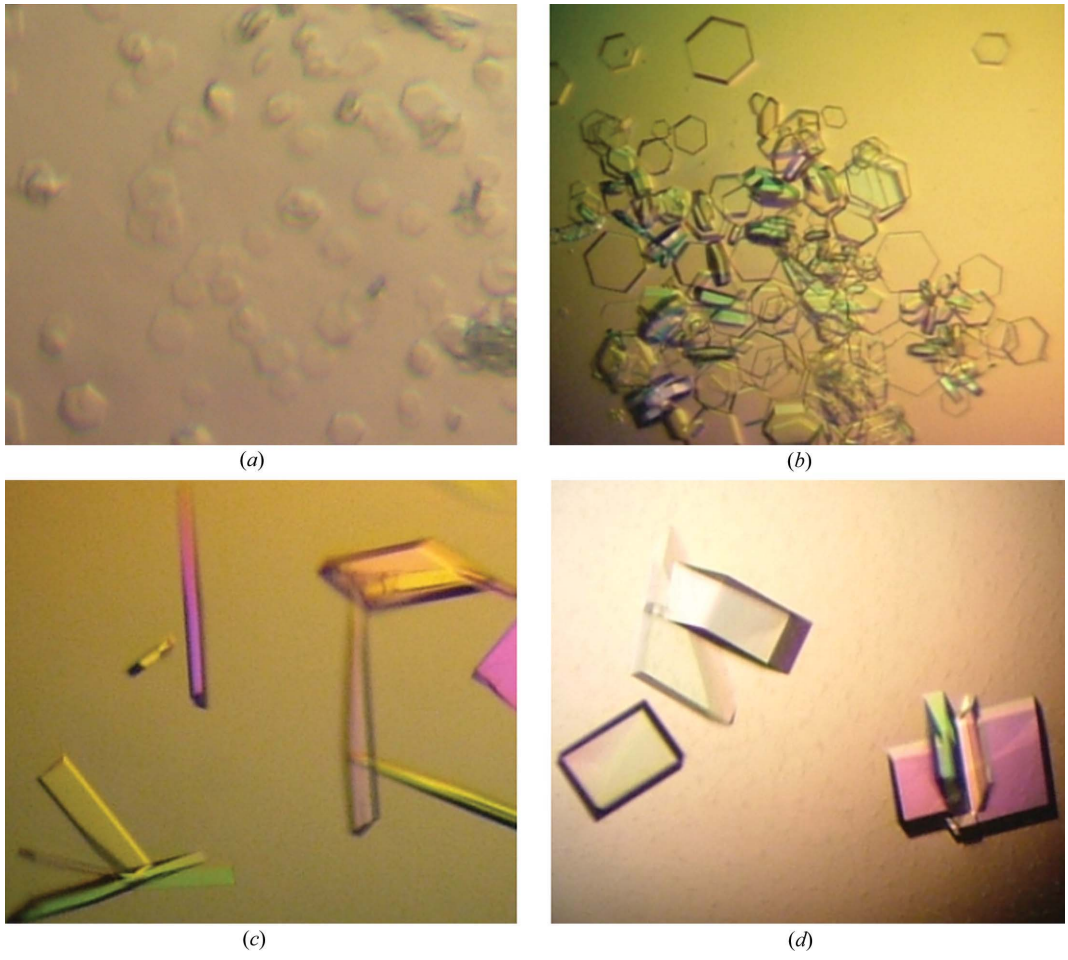

Figure 3
Crystals of GKAP GH from *R. norvegicus*. (*a*) Microcrystal of GKAP GH fragments grown in 0.1 *M* MES pH 6.0, 2.0 *M* ammonium sulfate. (*b*) Crystals of GKAP GH (residues 807–971, Δ917–945) grown in 0.1 *M* MES pH 6.0, 12.5% PEG 4000, 0.2 *M* ammonium sulfate with a typical size of 0.1 × 0.02 × 0.02 mm. (*c*) Crystals of MBP1 (residues 28–389)-GKAP GH (residues 807–971, Δ917–945) were grown in 0.1 *M* sodium citrate pH 5.0, 10% PEG 1500, 0.1 *M* NaCl with a typical size of 0.2 × 0.05 × 0.02 mm. (*d*) Crystals of MBP2 (residues 28–387)-GKAP GH (residues 807–971, Δ917–945) with a size of 0.2 × 0.2 × 0.1 mm were grown in 0.1 *M* sodium citrate pH 5.0, 10% PEG 1500, 0.1 *M* NaCl.

The MBP fusion provided an additional advantage in determining phase information by molecular replacement. Two copies of MBP were found in the asymmetric unit by *MOLREP* using an open conformation of MBP as a search model (Sharff *et al.*, 1992). The top two solutions with peaks of 8.02σ and 7.94σ in a rotational search were two times higher in peak height than the other solutions. The phases were further improved by density modification using *CNS* (Brünger *et al.*, 1998) and the resulting electron-density map with a figure of merit of 0.78 was readily interpretable. Two molecules of MBP-GKAP were clearly visible in the electron-density map (Fig. 5). Model building and structure refinement of the model are currently under way. The forthcoming MBP-GKAP structure will provide key information for the structural understanding of the GH domain that is conserved in GKAP family proteins. This study suggests that the truncation of disordered loops and the fusion of target proteins to globular proteins with a short connecting linker could serve as

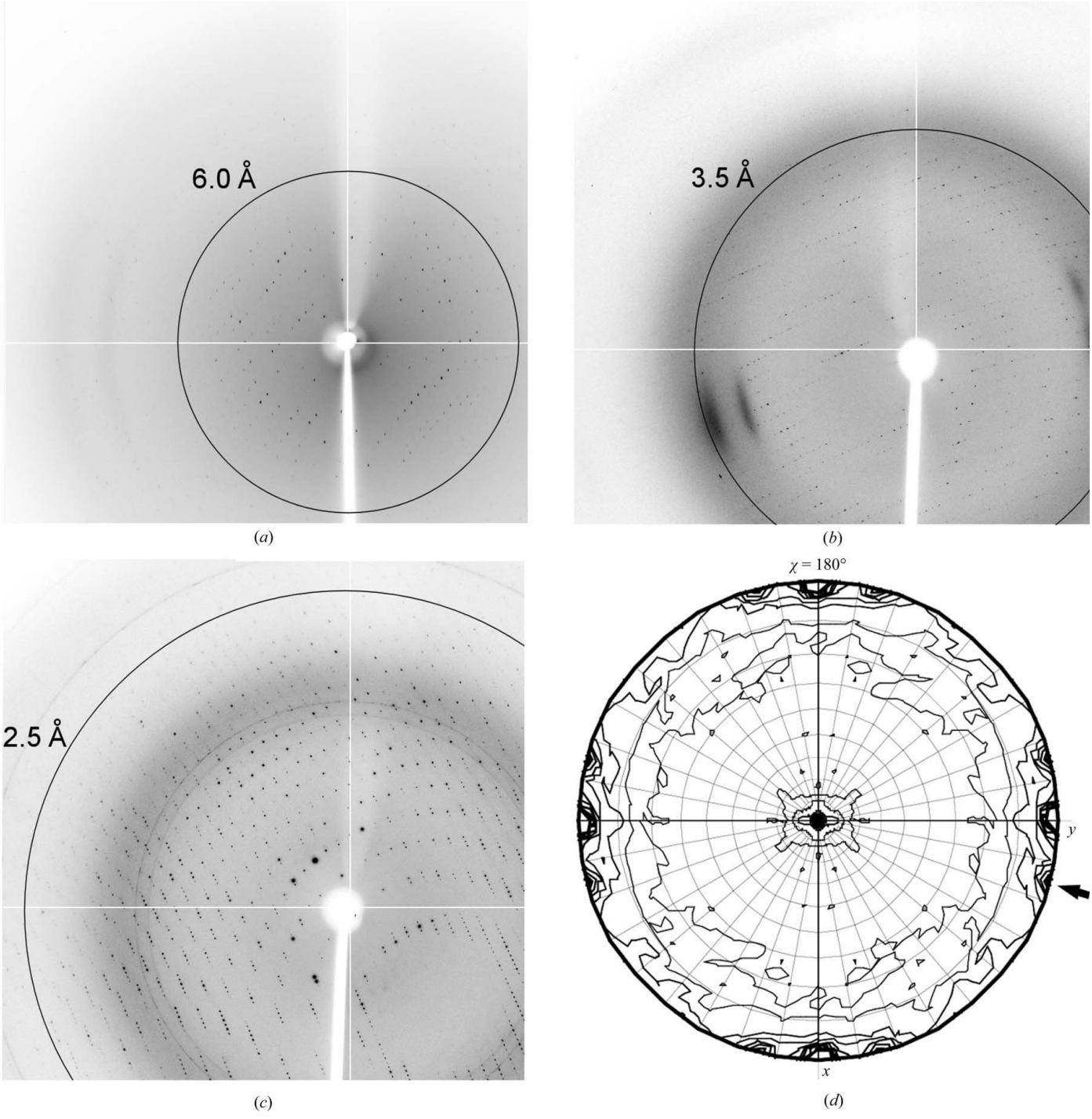

Figure 4
Diffraction images of GKAP GH crystals. (*a*) A diffraction image of a GKAP GH crystal (residues 807–971, Δ917–945). (*b*) A diffraction image of an MBP1-GKAP GH crystal. (*c*) A typical diffraction image of an MBP2-GKAP GH crystal. (*d*) Self-rotation function for MBP2-GKAP GH in the $\kappa = 180^\circ$ section calculated with *MOLREP* using default parameters, with a search radius of 27.5 Å and data in the resolution range $9.0 > d > 3.5$ Å. The arrow indicates one of the twofold NCS peaks.

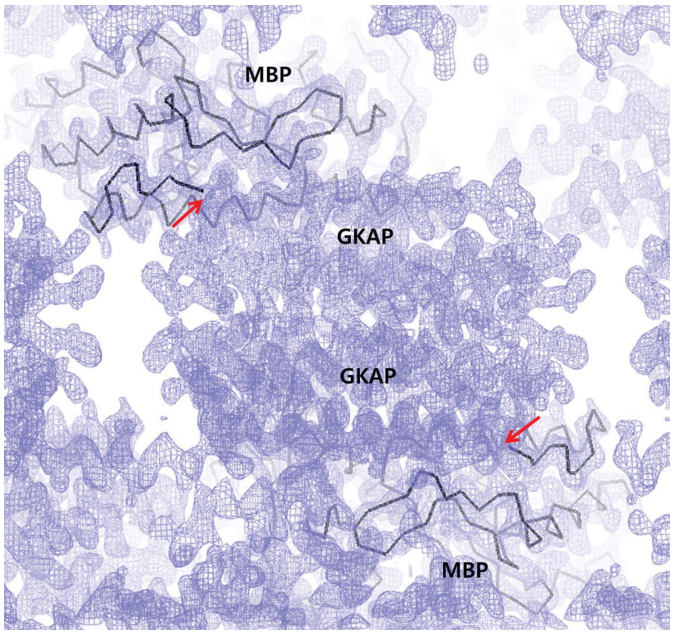

Figure 5
Density-modified electron-density map showing MBP-GKAP molecules. The phase information was obtained from the partially built MBP-GKAP model. The electron-density map was calculated with a resolution cutoff of 4.0 Å to show molecular envelopes. The C^{α} traces for MBP molecules are shown as black lines. Red arrows indicate the start of GKAP electron densities.

alternative methods in optimizing constructs for crystallization when traditional approaches have failed to yield good crystals.

We would like to thank the beamline staff at PLS-5C and PLS-7A at the Pohang Accelerator Laboratory. This project was supported by a National Research Foundation of Korea (NRF) grant (No. 2011-0025110) to YJI and the Intramural Research Program of Chonnam National University to YJI (2011).

References

Brünger, A. T., Adams, P. D., Clore, G. M., DeLano, W. L., Gros, P., Grosse-Kunstleve, R. W., Jiang, J.-S., Kuszewski, J., Nilges, M., Pannu, N. S., Read, R. J., Rice, L. M., Simonson, T. & Warren, G. L. (1998). *Acta Cryst.* D**54**, 905–921.
Hirao, K., Hata, Y., Ide, N., Takeuchi, M., Irie, M., Yao, I., Deguchi, M., Toyoda, A., Sudhof, T. C. & Takai, Y. (1998). *J. Biol. Chem.* **273**, 21105–21110.
Hung, A. Y., Sung, C. C., Brito, I. L. & Sheng, M. (2010). *PLoS One*, **5**, e9842.
Kim, E., Naisbitt, S., Hsueh, Y.-P., Rao, A., Rothschild, A., Craig, A. M. & Sheng, M. (1997). *J. Cell Biol.* **136**, 669–678.
Manneville, J. B., Jehanno, M. & Etienne-Manneville, S. (2010). *J. Cell Biol.* **191**, 585–598.
Matthews, B. W. (1968). *J. Mol. Biol.* **33**, 491–497.
Moon, A. F., Mueller, G. A., Zhong, X. & Pedersen, L. C. (2010). *Protein Sci.* **19**, 901–913.
Naisbitt, S., Kim, E., Tu, J. C., Xiao, B., Sala, C., Valtschanoff, J., Weinberg, R. J., Worley, P. F. & Sheng, M. (1999). *Neuron*, **23**, 569–582.
Naisbitt, S., Kim, E., Weinberg, R. J., Rao, A., Yang, F.-C., Craig, A. M. & Sheng, M. (1997). *J. Neurosci.* **17**, 5687–5696.
Naisbitt, S., Valtschanoff, J., Allison, D. W., Sala, C., Kim, E., Craig, A. M., Weinberg, R. J. & Sheng, M. (2000). *J. Neurosci.* **20**, 4524–4534.
Otwinowski, Z. & Minor, W. (1997). *Methods Enzymol.* **276**, 307–326.
Sharff, A. J., Rodseth, L. E., Spurlino, J. C. & Quiocho, F. A. (1992). *Biochemistry*, **31**, 10657–10663.
Sheng, M. & Hoogenraad, C. C. (2007). *Annu. Rev. Biochem.* **76**, 823–847.
Shin, S. M., Zhang, N., Hansen, J., Gerges, N. Z., Pak, D. T. S., Sheng, M. & Lee, S. H. (2012). *Nature Neurosci.* **15**, 1655–1666.
Smyth, D. R., Mrozkiewicz, M. K., McGrath, W. J., Listwan, P. & Kobe, B. (2003). *Protein Sci.* **12**, 1313–1322.
Tu, J. C., Xiao, B., Naisbitt, S., Yuan, J. P., Petralia, R. S., Brakeman, P., Doan, A., Aakalu, V. K., Lanahan, A. A., Sheng, M. & Worley, P. F. (1999). *Neuron*, **23**, 583–592.
Vagin, A. & Teplyakov, A. (2010). *Acta Cryst.* D**66**, 22–25.
Winn, M. D. *et al.* (2011). *Acta Cryst.* D**67**, 235–242.